

Completion of the AMR-C Instrument for Sentinel-6

Frank Maiwald , Senior Member, IEEE, Shannon T. Brown, Timothy Koch, Lance Milligan, Pekka Kangaslahti, Erich Schlecht, Member, IEEE, Anders Skalare, Matthew Bloom, Violet Torossian, John Kanis, Shannon Statham, Shawn Kang, and Parag Vaze

Abstract—The advanced microwave radiometer-climate quality (AMR-C) is a part of the European Sentinel-6A/B series, a collaboration between ESA and NASA, of two Earth-observing satellites, which will be launched in 2020 and 2025. Compared to its predecessor, Jason-3, the two AMR-C radiometer instruments have an external calibration system which enables higher radiometric stability accomplished by moving the secondary mirror between well-defined targets. Sentinel-6 allows continuing the study of the ocean circulation, climate change, and sea-level rise for at least another decade. Besides the external calibration for the AMR heritage radiometer (18.7, 23.8, and 34 GHz channels), the AMR-C contains a high-resolution microwave radiometer (HRMR) with radiometer channels at 90, 130, and 168 GHz. This subsystem allows for a factor of $5\times$ higher spatial resolution at coastal transitions. This article presents a brief description of the instrument and the measured performance of the completed AMR-C-A and AMR-C-B instruments.

Index Terms—Earth observation, internal and external noise source, microwave radiometer, radiometer performance.

I. INTRODUCTION

THE development of the AMR instruments started in 1992 with TOPEX/Poseidon [1], followed by Jason-1 in 2001 [2], and OSTM/Jason-2 in 2008 [3] (see Fig. 1). The only active mission today is Jason-3, which was launched in 2016 [4]. With Sentinel-6A/B, the measurements will continue for an additional decade allowing more precise studies of the rate of sea-level rise (see Fig. 2), including observations of any change in that rate. So far, the results of the missions mentioned above show a (3.1 ± 0.4) mm/year increase in sea level. It is crucial to understand the timeline when predicting the impact on the coastal regions so that the affected communities can implement countermeasures.

The Sentinel-6 instrument platform consists of the next generation of Ku/C-band radar altimeter, Poseidon-4 [6], and the improved AMR-C instrument, both increasing spatial resolution. Furthermore, there is a set of instruments for precise orbital determination: GNSS-RO, Laser Reflector Array, DORIS, and GNSS-POD [7].

Manuscript received January 22, 2020; revised April 21, 2020; accepted April 26, 2020. Date of publication May 6, 2020; date of current version May 15, 2020. This work was supported by the Jet Propulsion Laboratory, California Institute of Technology, and funded by the National Aeronautics and Space Administration under Grant 80NM0018D0004. (Corresponding author: Frank Maiwald.)

The authors are with the Jet Propulsion Laboratory, California Institute of Technology, Pasadena, CA 91106 USA (e-mail: frank.maiwald@jpl.nasa.gov; shannon.brown@jpl.nasa.gov; timothy.koch@jpl.nasa.gov; lance.milligan@jpl.nasa.gov; pekka.kangaslahti@jpl.nasa.gov; erich.schlecht@jpl.nasa.gov; anders.skalare@jpl.nasa.gov; matthew.bloom@jpl.nasa.gov; violet.torossian@jpl.nasa.gov; john.kanis@jpl.nasa.gov; shannon.statham@jpl.nasa.gov; shawn.kang@jpl.nasa.gov; parag.vaze@jpl.nasa.gov).

Digital Object Identifier 10.1109/JSTARS.2020.2991175



Fig. 1. Past and future series of altimeter experiments.

Unlike Jason-3, the AMR-C has a mechanism to calibrate the low-frequency radiometer between two targets with known temperatures, a hot target at about room temperature and a cold target at 3 K implemented with a mirror looking into cold space. This calibration system, called the supplemental calibration subsystem (SCS), allows AMR to meet the stringent Level 1 (L1) requirements to correct the wet tropospheric path delay over a range of 0–40 cm with an error less than 1 cm over one year with long-term stability of 0.7 mm. This imposes an instrument error requirement of less than 0.9 K (0.65 K in Table V is allocated to the instrument) error for the AMR radiometer with ± 0.1 K calibration error, which can only be obtained from the SCS.

To support the high-mode resolution from the radar altimeter, the experimental high-resolution microwave radiometer (HRMR) subsystem allows for high spatial resolution at coastal transitions to 5 km compared to 25 km for the AMR

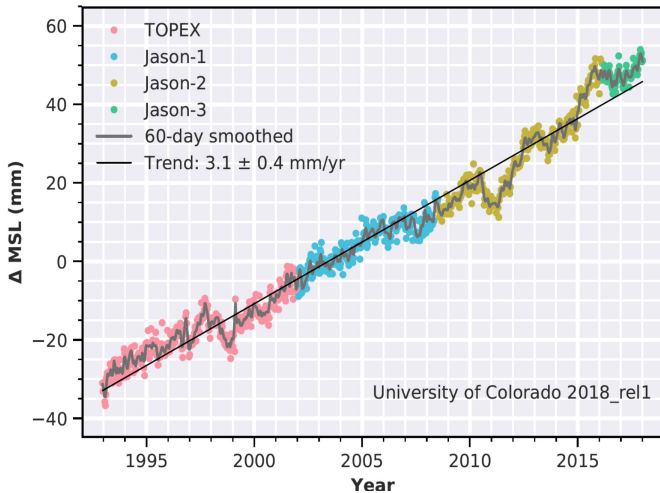


Fig. 2. Global mean rise of sea-level over time (removed are the seasonal variation of ± 7.5 mm) from TOPEX throughout Jason-3 [5].

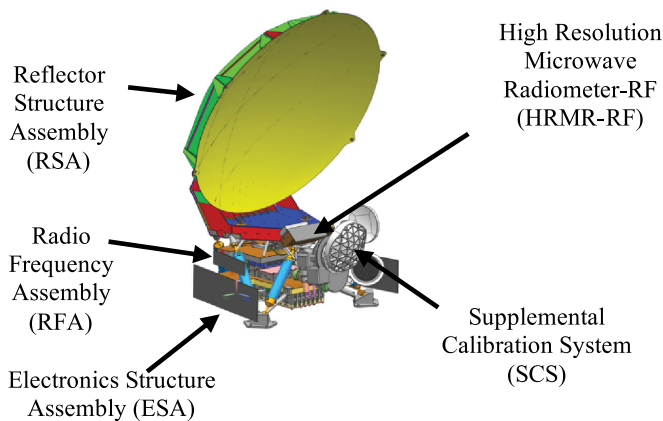


Fig. 3. AMR-C instrument model with its main subsystems.

radiometer. No science requirements were applied to HRMR because it was implemented as a technology demonstration. We will describe the AMR and HRMR subsystems, including their measured performance for both AMR-C instruments, AMR-C-A and AMR-C-B, in the following sections.

II. INSTRUMENT DESCRIPTION AND DEVELOPMENTS

AMR-C (see Fig. 3) can be broken down into five major subsystems: the reflector structure assembly (RSA) made out of carbon-fiber which was built by Orbital-ATK, the radio frequency assembly (RFA), electronics structure assembly (ESA), the supplemental calibration system (SCS, see Fig. 4), including the launch lock mechanism (LLM) and the standard dual-drive actuator (SDDA), which was built by honeybee robotics, and the HRMR. The ESA includes dual redundant RF assemblies and electronics units (EUs) for the AMR radiometer.

A challenge was the coordination of two significant efforts: the structural analyses and the thermal design. The structural efforts were more complicated than expected due to the resonant coupling of all subsystems, which was compounded by the early design decision to adopt the Jason-3 bipods made from

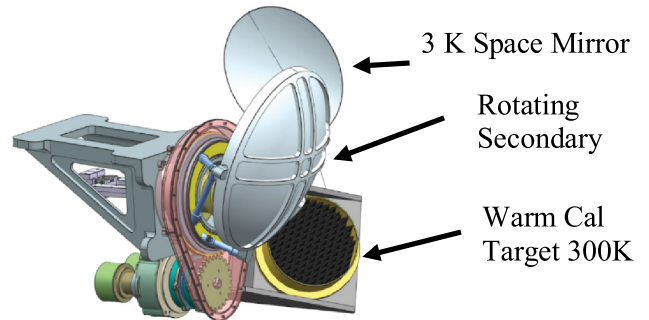


Fig. 4. SCS contains the LLM, which constrains the movement of the secondary mirror during launch, and the SDDA, which contains a redundant actuator with a gearbox.

carbon fiber (light blue in Fig. 3), which attaches AMR-C to the spacecraft deck. One advantage of this design is good thermal insulation between the instrument and the spacecraft, which allowed optimization of the internal thermal design of the instrument. One significant result was the inclusion of two sets of radiators connected to the ammonia filled redundant heat pipes embedded in the RFA and ESA panels.

Changes from the Jason-3 thermal design were needed due to the inclusion of the SCS and HRMR subsystems. These new subsystems did not allow a symmetrical arrangement of the electronic boxes in the center of the instrument, which would have provided thermal stabilization with a single passive radiator as for Jason-3. This resulted in the conductive and radiative separation of the temperature-sensitive RF electronics (which have a stringent stability requirement) from the power, telemetry, and processing electronics. This separation allowed minimization of the required heater power with high stability < 0.04 K/min and control ability throughout the lifetime of the RF electronics. The passive thermal design consists of multilayer insulation (MLI) and single-layer insulation (SLI) to insulate the instrument radiatively from the space environment, conductive decoupling by struts and blades, AgFEP (silver Teflon) taped radiators, and black and gold anodization to achieve the required optical properties on exterior surfaces. The active thermal design consists of seven nominal and five redundant proportional-integral-derivative (PID) controlled operational heater loops to provide the required temperature stability. Two heater loops are operated for the temperature-sensitive RF hardware (AMR and HRMR RF) with 2-Hz loop bandwidth. All other heater controllers have 0.25 Hz bandwidth. These PID control loops have been verified first with a breadboard setup. The final verification of the loops on the instrument level was performed during the instrument integration and test (I&T) thermal vacuum tests for both instruments. For nonoperational modes, six nominal and five redundant survival heaters are installed, each controlled by two thermostats in series.

In order to ensure seamless integration of AMR-C onto the spacecraft, the thermal control algorithm was defined and agreed by all key players (JPL, ESA, and airbus) very early in the development. Furthermore, the control parameters were adjusted after completing the instrument I&T activities for successive thermal tests at spacecraft level.

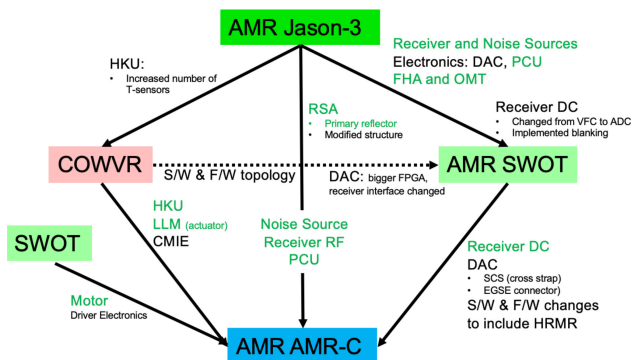


Fig. 5. Utilization of existing components (green) and electronics from predecessor flight projects: Jason-3, COWVR, and SWOT. Minor changes on HKU and DAC layout were implemented. The change from VFC's to ADC's required changing the firmware.

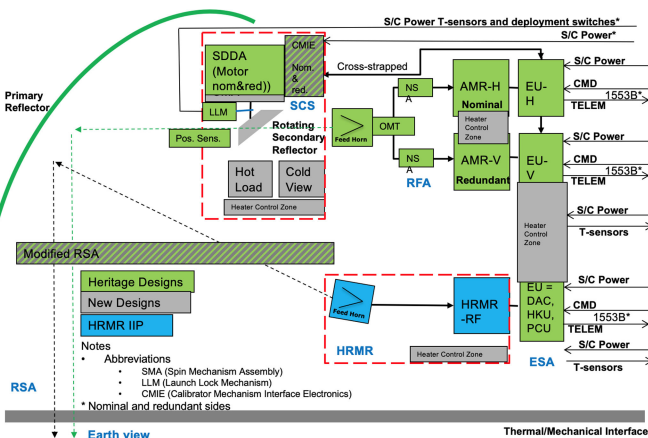


Fig. 6. Simplified block diagram of AMR-C.

The design of AMR-C began approximately one year later than the rest of the spacecraft. This situation required a very early definition of the mechanical, thermal, structural, and electrical interfaces with the spacecraft provider airbus. The initial interface definition relied on using the existing electronic designs with minimal changes (see Fig. 5) and heavily reuse documentation and assembly processes.

For the new HRMR subsystem, the team adopted the existing interfaces between the RF modules and the EU electronics, comprised of power supplies, temperature sensors, data processing, firmware (FW), and flight software (FSW). FW and FSW were modified to keep all the controlling electronics interchangeable. Reuse of the existing electronics designs from earlier projects greatly helped streamline the implementation.

The main instrument of AMR-C (see Fig. 6) is the low-frequency AMR radiometer with its three channels at 18.7, 23.8, and 34 GHz. A movable secondary mirror focuses the signal into a circular feedhorn assembly (FHA), where it is split by an orthomode transducer (OMT) into the two principal polarizations, which are coupled to a primary receiver side and a redundant (cold spare) one.

Each receiver has three independently controlled diode noise sources for internal calibration. Fig. 7 shows the block diagram

of the receivers. The signal is split into 18/24 GHz and 34 GHz bands, which go to p-i-n-diode switches that provide gain stability by switching to the receiver inputs between the antenna and the fixed load at a known temperature (Dicke switching). Each amplification chain, a cascade of amplifiers and filters, has sufficient signal gain for detection with a tunnel diode. The detector voltage output signal is amplified and then digitized by an ADC that is read by an FPGA.

The digital processing is performed in the data acquisition and control (DAC) unit, which controls the entire instrument. The DAC and all other electronics obtain their power from the power converter unit (PCU). All temperature sensors are selected and read by the housekeeping unit (HKU). The three units DAC, PCU, and HKU together form the electronics unit (EU).

The primary and redundant EU were cross strapped to two control motor interface electronics (CMIE) units to ensure full electronic redundancy for both motors in the SDDA that moves the secondary mirror.

An 8-bit microcontroller running at 12 MHz with limited memory and no operating system was used as the core processing and command and data handling system. The simple philosophy applied to the FSW architecture by using interrupt-driven control and timers allowed precise movement of the SCS. The interrupt priority assigned to the controller allowed the deterministic and precise timing of the service handlers. All interrupts are synchronized to the 12 MHz system clock. A custom watchdog circuit allowed re-initialization of the DAC in the event of nonrecoverable failure without power cycling the instrument. The robust design also enables updating the FSW in flight. The DAC processes the data stream and transfers the data package to the spacecraft data bus using MIL-STD-1553B protocol.

While the radiometer operates, the SCS can be activated to perform an external calibration between two stable loads, one at approximate room temperature and the other at 3 K from cold space. With these two loads, AMR can be swiftly and accurately calibrated without changing the orientation of the entire spacecraft to point at the cold sky or waiting for passage over a known target on Earth. The purpose of the SCS is to provide long-term calibration stability to detect minute long-term sea-level variations. The estimate is that the internal noise diodes provide sufficient calibration stability to measure these minute variations for five days of operation, which is consistent with previous instruments (Jason-3). The result is improved instrument accuracy. More details on the instrument are provided in [8].

The readout of the radiometer channel data from Jason-3 utilized voltage-to-frequency converters (VFC) that were replaced by analog to digital converters (ADC) with 18-bit resolution. Choosing the ADC removes the reported [4] “flat spots” in the radiometric data caused by harmonic locking of the VFC. The ADCs also resulted in reduced backend noise. We applied the same assembly processes for all RF circuits, which were developed for Jason-3 [4].

As mentioned earlier, changes were made to the instrument FSW and FW for SCS and HRMR. Due to the increased functionality of the SCS and receivers, the control FPGA was

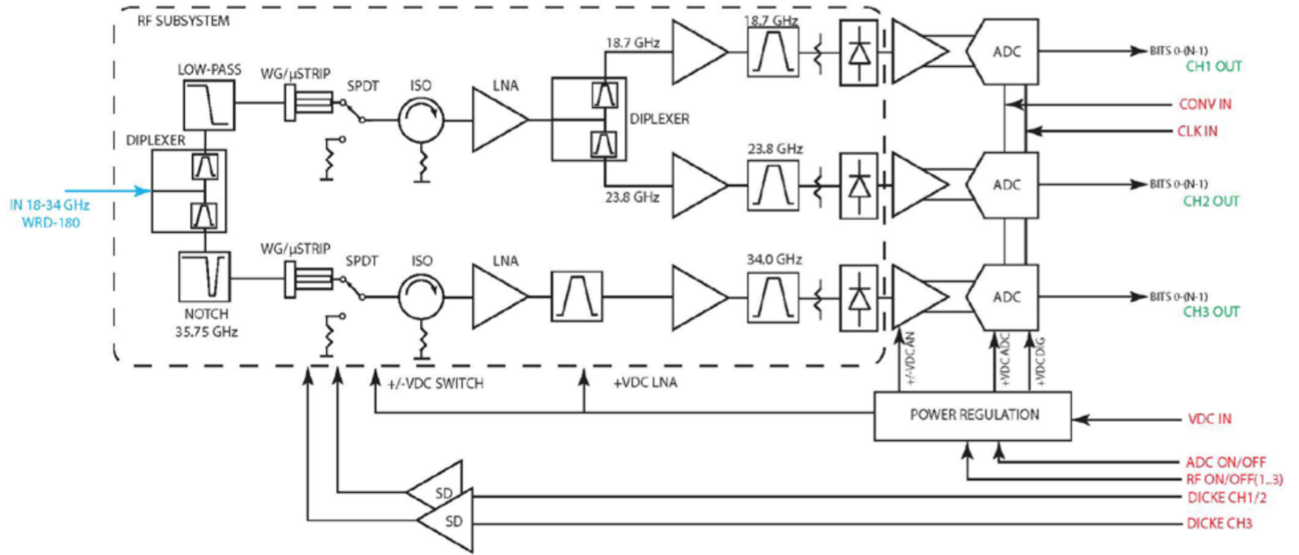


Fig. 7. AMR receiver block diagram. Starting from the left, the waveguide transitions (diplexer to microstrip lines), Dicke switch, isolator, LNAs and filter stages, detectors, and backends with drivers/ADCs and their interfaces are displayed. The signal is split into three bands. An FPGA controls and reads out the measured signal every 1/16 of a second. The HRMR topology is very similar [8].

upgraded to the larger microsemi RTSX72SU, from the same family used in Jason-3. The impact on the FPGA code was minimal: implementation of readout topology for digital receiver backends and more inputs/outputs for the calibration mechanism interface electronics (CMIE). In addition, fast switching (2 kHz) of the HRMR Dicke switches reduces the $1/f$ noise from prototype measurements to the flight implementation by a factor of 25 at 60 s time scale. This noise level enables 0.2 K radiometric stability (see Table III) over 60 s. The FSW design changes include control and telemetry of the secondary mirror position, faster ADC readouts for HRMR, and selectable combinations of internal thermistors to optimize calibration.

HRMR must share the primary reflector with AMR. Off-axis operation at higher frequencies results in worse beam distortion, so the HRMR must be on the primary optical axis.

Results from optical simulations and the successive beam pattern measurements (including cold 3 K space mirror) confirmed that the impact on the beam performance of the AMR radiometers was acceptable as per our instrument science model and that the primary reflector surface roughness of better than $23 \mu\text{m}$ RMS was sufficient to support the high frequencies. As shown in Fig. 8, the beam performance of AMR has good symmetry down to -15 dB, even when the AMR beam is not in the optical center of the primary reflector with the measured offset of $(-0.5, -0.5)$ degrees. However, the alignment of the AMR-C instrument with respect to the altimeter is defined by the AMR beam and can be compensated by the shimming of the entire instrument. As a result, the HRMR beam points along-track 3.4° ahead of AMR, which can be corrected during the data processing, assuming the atmospheric conditions do not change significantly during the time (1.06 min at a 1336 km altitude) between both beams point at the same location.

The detailed structural, thermal, optical, and performance (STOP) analysis was critical to evaluate the pointing performance and to verify that the instrument stays within alignment

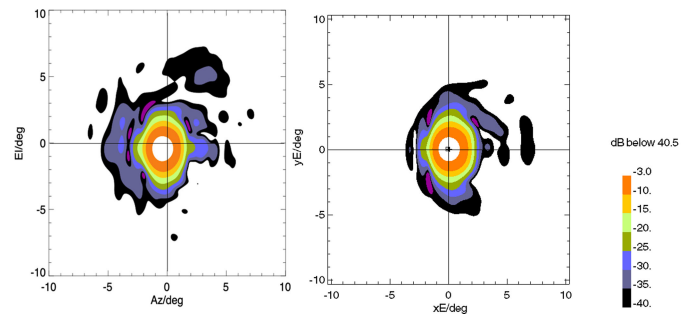


Fig. 8. Beam pattern of 18.7 GHz measured left, calculated right.

allocations under the expected conditions. Multiple factors that could affect the alignment are: Prelaunch: bias/drift during installation resulting in uncertainty of the boresight; residual error introduced during installation onto the spacecraft; secondary repositions of the movable reflector when it hits the hard stops; Postlaunch: on-orbit bias/drift of gravity; hygroscopic changes in the carbon fiber structures; and during launch bolted joint slip and thermo-elastic distortion.

The accuracy of the STOP analysis was verified by thermal balance tests, dynamical tests that confirmed the structural model, and the antenna beam pattern measurement, which confirmed the calculated predictions. Final calibration tests will be conducted on orbit.

III. INSTRUMENT PERFORMANCE

In this section, we provide the performance data of the two AMR-C instruments. Each RF component was measured, compliance with requirements verified, and the data inserted into our instrument performance model. The beam pattern was measured in the near-field, analyzed, and verified with an optical

TABLE I
PERFORMANCE VERIFICATION OF AMR-C THERMAL DESIGN
FOR BOTH INSTRUMENTS

Requirement	AMR-C-A Launch 2020	AMR-C-B Launch 2025	Comment
Stability of receivers $\Delta T/\Delta t < 0.1^\circ\text{C}/10$ min	$<0.1/10$ min(*)	$<0.1/10$ min(*)	RSA, HRMR, w/g, FHA
Orbit Averaged Operational Heater Power < 35 W	26	26	All heaters
Functionality (PID, control authority, survival)	verified	verified	Final control values
Stability of RF elements $<0.04\text{K}/\text{min}$	$<0.04\text{K}/\text{min}$	$<0.04\text{K}/\text{min}$	Low noise
Stability of calibration targets $<0.06\text{K}/\text{min}$	$<0.01/\text{min}$	$<0.01/\text{min}$	Stable reference

(*) Verified in radiometric calibration phases of the AMR-C FM-A and -B TVAC tests.

TABLE II
LEVEL 5 AMR INSTRUMENT REQUIREMENTS

Requirements, over science temperature 15 to 50°C	AMR- C-A	AMR- C-B	Comment
Input Return Loss ≥ 15 dB	≥ 15	≥ 15	as expected
Dicke Switch Isolation ≥ 30 dB	≥ 30	≥ 30	as expected
Frequency and bandpass	verified	verified	
Stopband Rejection > 50 dB	> 50	> 50	as expected
System Noise Figure ≤ 6.6 dB	≤ 5.7	≤ 5.9	
System gain/temperature ≤ 0.2 dB/ $^\circ\text{C}$	≤ 0.1	≤ 0.1	
ADC noise $< 1/3$ of radiometer noise	$<1/9$	$<1/10$	digitizer only
Dynamic range 2.7 to 750 K	verified	verified	
NEDT at 1Hz < 0.2 K	<0.13	<0.2	

In total, five radiometer systems were built, two for each AMR-C and one spare. Each of these radiometers performed within requirements. Insignificant deviations in noise figure, gain, and NEDT were observed over 15– 50°C , which reflect the variation at the component level.

propagation model, which includes the thermal and gravitational distortions.

A. Instrument Thermal Design

The thermal design and modeling were verified through measurements during the I&T phase (see Table I) and the test results were used to correlate the thermal model. The optimized PID parameters of the heater control loops showed good agreement with the predicted ones. The thermal vacuum (TVAC) test results and the final thermal flight predictions from the correlated thermal math model confirmed full compliance with the operational and nonoperational temperature limits and with the thermal stability requirements in all on-orbit extreme cases. This was verified for both the instruments, AMR-C-A and AMR-C-B.

B. AMR Receiver Performance Results

The receiver performance (see Table II) was consistent with that achieved for the Jason-3 receivers. The linearity was measured using the constant deflection technique. The error due to receiver nonlinearity is less than 0.1 K for all channels.

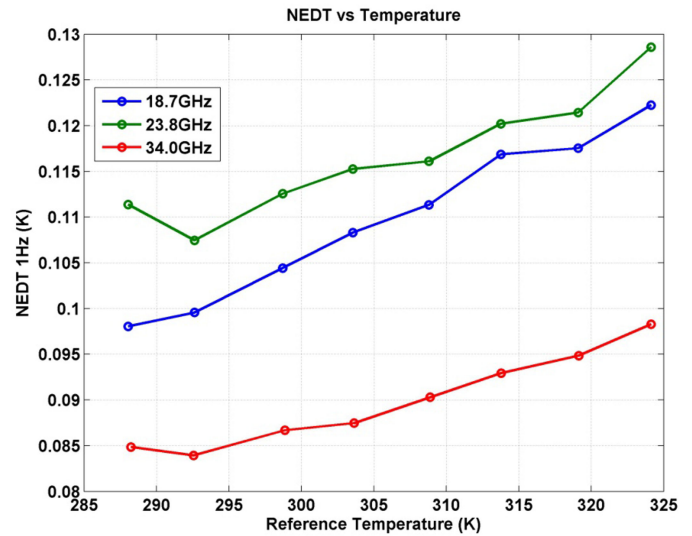


Fig. 9. Measurement noise versus receiver temperature measured at the reference load for AMR (primary side shown only).

The modified digital backend did not degrade the performance. The measurement noise is computed from the thermal-vacuum data as a function of the Dicke reference load temperature, while the radiometer is viewing a cold calibration target. It is computed by finding the sample standard deviation of successive triplets of calibrated antenna temperatures and averaging those independent but noisy samples over each 3 min dwell. This noise will always be higher than the theoretical white noise limit as it contains the noise from the calibration measurements. An example of the measurement noise is shown in Fig. 9.

The increase of the receiver noise temperature with increasing receiver physical temperature is the dominant term controlling the variation of the measurement noise with temperature. The receiver noise temperature at the input of the diplexer is in average 1000 K (better for 18.7 GHz and increasing from 23.6 to 34 GHz) for AMR, meaning the variation in NEDT over the full range of Earth data (120–300 K) is smaller than $\pm 10\%$.

C. HRMR Receiver Results

The HRMR [8], [9] was included in the AMR-C instrument as a technology demonstration that provides a $5\times$ higher-spatial resolution, resulting in improved accuracy of science data in the coastal transitions. The science goals were nonbinding requirements for HRMR and the measured performance was better than expected. We demonstrated that a technology demonstration could be accommodated with a limited impact on the overall instrument integration. Furthermore, reusing existing electrical and optical interfaces allowed for rapid integration. In operation, HRMR data will not use the calibration targets of the SCS. This subsystem will be cross calibrated based on the AMR measurements before coastal transitions occur. This approach is supported by internal Dicke switching, which provides the required gain stability over 60 s with internal noise diodes. Due to its low-noise InP amplifiers [10], the HRMR had a sensitivity

TABLE III
HRMR RECEIVER DESIGN PARAMETERS

Requirements, 15 to 45C science temperature range	AMR-C-A	AMR-C-B
Center Frequency	verified	verified
Bandwidth <6 GHz	< 6	< 6
System Noise Figure $K \leq 3500$ @168 GHz	3240	≤ 3500 @20°C
System gain/temperature ≤ 0.2 dB/°C	≤ 0.2	≤ 0.2
NEDT at 1Hz <0.2K	<0.17K	<0.13K

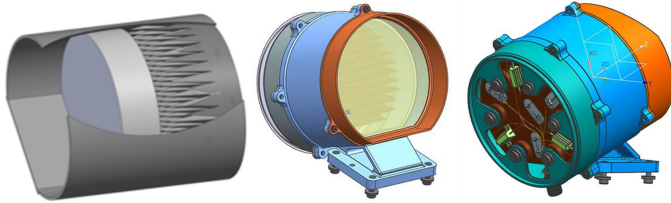


Fig. 10. Warm calibration target: UV and IR blocking shield and 25.8-mm-thick EPS radome, microwave calibration target with 1.1-mm-thick Eccosorb CF117 on an aluminum pyramidal structure.

(NEDT) of better than 0.2 K and stability for over 60 s to 0.2 K for all three frequencies (see Table III).

D. Warm Calibration Target

The purpose of the Warm calibration target (WCT) (see Fig. 10) is to provide AMR-C with a near room temperature reference load, to aid in precise characterization over longer time spans (≈ 1 year) of the calibration noise diodes that are used during the science data collection. The requirement is an RMS radiometric brightness uncertainty of 0.2 K in a single calibration instance, which is derived from a requirement on the RMS science data uncertainty during a one-year period with the assumption of one calibration performed every five days in Earth shadow. While the WCT should meet this requirement, performance can be improved by performing calibrations as often as every two days. In addition, there will be an on-orbit calibration process where AMR-C will be pointed to “stare” at the WCT for an extended time, through correlation of the measured WCT brightness temperatures to the physical temperatures of temperature sensors installed inside the WCT (>10 PRTs). It should be noted that the requirement is not an accuracy requirement but a repeatability requirement since WCT will be used only to determine long-term parameter drift in the AMR-C instrument. The largest uncertainty in the WCT brightness temperature is expected to be variations in infrared heat loading caused by variations in Earth’s albedo due to clouds.

The calibration target consists of an aluminum plate with an array of square pyramids with a height of 34 mm and a period of 8.6 mm, which is coated by a 1.1-mm-thick layer of Eccosorb CR-117 microwave absorber, a castable plastic resin with a filling of iron dust. The return loss was calculated with an electromagnetic field simulator (Ansys HFSS) to be higher than 50 dB in all three AMR-C bands, and this was also confirmed

TABLE IV
MAIN PARAMETER OF AMR-C FOR SPACECRAFT INTERFACES

Requirement	AMR-C-A (CBE)	AMR-C-B (CBE)	Comment
Operational Power (W)	50.7	50	Allocation of 76 W
Survival power (W)	34.8	33.4	Including HRMR
Mass (kg)	58.2	58.3	Allocation of 65 kg
Power (W) HRMR	12.4	12.6	HRMR only
Mass (kg) HRMR	3.2	3.3	no cables
Data rate	3.1 kbps	3.1 kbps	Fixed for each EU

through measurements on the delivered hardware. The design of the calibration target is based on reference [11].

The pyramids are machined into an aluminum blank using “plunge” electrical discharge machining, and this “pyramid plate” is then used to create a negative mold from a rubber material, after which the microwave absorber layer is created between the plate and rubber mold in a vacuum injection molding process.

The largest uncertainty in the WCT brightness temperature is due to infrared heat loading of the poorly heat sunk microwave absorber tips at the top of the pyramids, and if left unchecked this could cause the brightness temperature and the PRT sensor temperatures to disagree by as much as 0.5 K (in a simulation, the absorber tips were sliced into nine layers and the microwave coupling to each layer and its temperature were first multiplied and the results added together for all layers to give the estimate). In order to meet the requirements, the WCT was, therefore, fitted with a 1-in-thick EPS Type IX [expanded polystyrene(EPS)] radome that by a conservative estimate will reduce both the IR heat load variations and the resulting increase of the brightness temperature uncertainty by a factor of four. During thermal vacuum ground testing of the radiometers, including the radome, no effects of the described type were actually seen. Exposure of EPS to UV results in surface yellowing so that increased heating from direct sunlight can cause the surface layer to soften and contract to release built-in stresses, so a UV/IR shield and a white-painted G-10 ring were added at the periphery of the radome to mitigate this effect.

Other contributions to the WCT brightness temperature uncertainty were estimated and found to be minor, such as antenna pattern spillover, pathlength variations due to thermal expansion/contraction, temperature gradients in the WCT aluminum plate, and losses in the EPS radome.

E. Instrument Performance and Calibration With SCS

Compared to Jason-3, the AMR-C instrument has nearly twice the mass and power requirements (see Table IV). Overall, the iterative optimization of the structural design showed that AMR-C of 58 kg is within the allowed structural design margins for the heritage bipod attachment to the spacecraft. We demonstrated margin against the design capability by analyses and tests. More importantly, the performance data of Jason-3 were repeated, which provides consistency when AMR-C replaces Jason-3.

Prelaunch test and analysis show that the AMR-C meets its key instrument performance requirement of 0.65 K allowable uncertainty in the brightness temperature (see Table V). The

TABLE V
CBE AT PRELAUNCH CALIBRATION ON SAMPLE ACCURACY (1 Hz) ERROR
BASED ON MODELING OF CALIBRATION MEASUREMENTS

TB sample accuracy error budget	AMR-C-A (CBE) [K]	AMR-C-B (CBE) [K]	Requirements [K]
Measurement noise	0.13	0.16	0.2 (sample in figure 9)
Antenna Temperature Calibration	0.2	0.21	0.5
Antenna Pattern Correction	0.1	0.1	0.2
Unallocated system margin	0.6	0.59	0.3
Total RSS	0.25 K	0.28 K	0.65K

There is a significant system margin for nominal and redundant AMR radiometer of both instruments AMR-C-A/B.

main contributions are measurement noise, antenna temperature calibration, and antenna pattern correction. The thermal-vacuum calibration test provided data needed to verify the first two allocations, and the antenna pattern correction allocation is verified by the analysis of the antenna range data. The results are summarized through the error budget in Table V, which has been updated based on the TVAC data analysis and antenna range validation tests.

The noise is found to be repeatable to less than 0.13 K across all channels for the nominal and redundant AMR sides. The worst-case bounding value for measurement noise is summarized in Table V. The antenna temperature calibration error is the residual of the path loss correction. The worst-case bounding TA calibration error across all channels was 0.2 K. The current best estimate (CBE) for the antenna pattern correction is based on the difference between the range measurement and the model, and the total error is estimated to be less than 0.1 K.

The AMR-C also has a new requirement to ensure the long-term stability of the path delay measurement to ± 1 mm over any one-year period. This translates to the requirement: The radiometer brightness temperature (TB) calibration shall be maintained to levels established during the cal/val phase with zero bias ± 0.1 K (standard deviation error) averaged over any one year period.

This requirement is met primarily by the uncertainty and stability of the external blackbody calibration targets viewed by the secondary calibration system motions. Each target is allocated 0.2 K of uncertainty each time it is observed, which is at least once every five days. However, the simulated (see Table VI) values of both targets show good agreement with the thermal vacuum tests. The 0.2 K TB uncertainty is a random residual error between independent target observations and does not include an absolute bias. Absolute biases of the optics are removed and validated during the commissioning phase by observing, ex., the cold sky mirror over land and ocean backgrounds. Any pickup of the side lobes which are not exposed to the cold sky is captured in the error term.

The calibration of AMR-C-A and -B agrees with the requirements. This concludes that both the instruments have similar performance characteristics and the external calibration allows for higher instrument stability, which in return enables monitoring of the sea-level change for more than a decade.

TABLE VI
CBE AT PRELAUNCH CALIBRATION ON RESIDUAL SEASONAL COMPONENT
ERROR; CBES SHOW MARGIN TO REQUIREMENTS

TB Stability Error Budget	AMR-C-A (CBE)	AMR-C-B (CBE)	Requirements [K]
Cold Target TB Uncertainty	< 0.14 K	< 0.15 K	0.2 K Sim. 0.2K
Hot Target TB Uncertainty	< 0.15 K	< 0.15 K	0.2 K Sim. 0.15K
Maximum Cold Target TB	~ 3 K 110K tested	~ 3 K 104K tested	100 K design but calibration at higher T
Minimum Hot Target TB	> 220 K	> 220 K	200 K
Internal Calibration RMS Stability	< 0.1 K	< 0.1 K	0.2 K
Calibration Frequency	Qualified to once every 2 days	Qualified to once every 2 days	At least once per 5 days
Antenna pattern correction (seasonal component)	< 0.03 K	< 0.03 K	0.03 K

Furthermore, the simulations on hot and cold targets show good agreement with the derived results from the thermal vacuum tests.

V. CURRENT STATUS AND FUTURE WORK

The reliable mixed RF and dc electronics developed for the Jason-3 project was successfully adapted for AMR-C, and the robust flight implementation approach has shown to significantly reduce schedule risks. The lessons learned from Jason-3, compact ocean wind vector radiometer (COWVR), and AMR-S have been applied and helped the team to meet or exceed the performance requirements and to deliver AMR-C-A on time to airbus, despite the significant schedule pressure. The second instrument, AMR-C-B, was well underway and went through the environmental tests and was delivered to airbus in December 2019. We successfully showed that a technology demonstrator, such as HRMR, could be included in a flight instrument with minor changes to existing interfaces. The exceptional performance of AMR and HRMR will enable quality sea-level height measurements with higher resolution also in coastal regions for the next decade.

ACKNOWLEDGMENT

The authors would like to thank the following team members for their on-going professional contribution to the project: the RF Assembly Team (M. Soria and H. Lim), the DC Assemblers (B. Drake and E. Hernandez), and the RF Test Team (H. Javadi, S. Sin, W. Chun, M. Chavez, and A. Pourangi), and E. Thiel for the assembly and delivery of the WCT. All these efforts together led to the successful delivery of the AMR-C instruments. They would also like to thank the contract partners Northrop Grumman Innovation Systems (former Orbital-ATK), Honeybee Robotics Spacecraft Mechanisms Corporation, and ZAX Millimeter Wave Corporation.

REFERENCES

- [1] C. S. Ruf, S. J. Keihm, and M. A. Janssen, "TOPEX/Poseidon microwave radiometer (TMR). I. Instrument description and antenna temperature calibration," *IEEE Trans. Geosci. Remote Sens.*, vol. 33, no. 1, pp. 125–137, Jan. 1995.

- [2] Y. Ménard *et al.*, "The Jason-1 mission special issue: Jason-1 calibration/validation," *Mar. Geodesy*, vol. 26, no. 3/4, pp. 131–146, Jul. 2003.
- [3] J. Lambin *et al.*, "The OSTM/Jason-2 mission," *Mar. Geodesy*, vol. 33, no. S1, pp. 4–25, Aug. 2010.
- [4] F. Maiwald *et al.*, "Reliable and stable radiometers for Jason-3," *IEEE J. Sel. Topics Appl. Earth Observ. Remote Sens.*, vol. 9, no. 6, pp. 2754–2762, Jun. 2016.
- [5] S. Nerem, Univ. Colorado. 2019. [Online]. Available: <http://sealevel.colorado.edu/>
- [6] M. Kuschnerus *et al.*, "Sentinel-6 Poseidon-4 RMC mode processing and expected performance," in *Proc. Oral Presentation Ocean Surface Topography Sci. Team Meeting*, 2018. [Online]. Available: https://meetings.avisio.altimetry.fr/?id=95&no_cache=1&tx_ausyclsseminar_pi2%5bobjAbstracte%5d=2473
- [7] 2019. [Online]. Available: <https://sealevel.jpl.nasa.gov/missions/jasoncs/>
- [8] J. L. Kloosterman *et al.*, "The advanced microwave radiometer-climate quality (AMR-C) instrument for sentinel-6," in *Proc. 28th Int. Symp. Space Thz Technol.*, Cologne, Germany, Mar. 13–15, 2017. [Online]. Available: <http://library.nrao.edu/issvt/catalog/2017000034>
- [9] P. Kangaslahti *et al.*, "High resolution microwave radiometer in AMR-C on sentinel-6," in *Proc 6th Workshop Adv. RF Sensors Remote Sens. Instrum., 4th Ka-Band Earth Observ. Radar Missions Workshop*, Nov. 11–13, 2019. [Online]. Available: <https://atpi.eventsair.com/QuickEventWebsitePortal/arsikeo/website>
- [10] X. Mei *et al.*, "First demonstration of amplification at 1 THz using 25-nm InP high electron mobility transistor process," *IEEE Electron Device Lett.*, vol. 36, no. 4, pp. 327–329, Apr. 2015.
- [11] S. Sandeep and A. Gasiewski, "Effect of geometry on the reflectivity spectrum of radiometer calibration targets," *IEEE Geosci. Remote Sens. Lett.*, vol. 11, no. 1, pp. 84–88, Jan. 2014.



Frank Maiwald (Senior Member, IEEE) received the Ph.D. degree in applied physics from I. Physikalisches Institute der Universität zu Köln, Cologne, Germany, in 1999.

In April 1999, he joined the Jet Propulsion Laboratory (JPL), Pasadena, CA, USA, as an ESA Post-doctoral Fellow. He was responsible for delivering space-qualified frequency multiplier chains for Herschel Space Observatory. Besides his interest in THz technology, he built radiometers and electronics for multiple space projects. His latest delivery was AMR-C-A instrument to the Sentinel-6 project. He is currently the Technical Group Supervisor of the Planetary Mass Spectrometry Team at JPL/NASA, working with a team of experts to deploy mass spectrometer instruments on future missions.

Dr. Maiwald is a senior member of the IEEE Microwave Theory and Techniques Society.



Shannon T. Brown received the B.S. degree in meteorology from Pennsylvania State University, Pennsylvania, PA, USA, the M.S. degree, and the Ph.D. degree, in 2005 both from the University of Michigan, Ann Arbor, MI, USA.

He joined the NASA Jet Propulsion Laboratory in Pasadena, CA, USA, in 2005 as a member of the engineering staff in the Microwave Advanced Systems section. He has been involved with the spaceborne Topex and Jason Microwave Radiometers, WindSat Polarimetric Radiometer, and the Jason follow-on

Advanced Microwave Radiometer. His research interests include microwave radiometer calibration, geophysical algorithm development for both passive and active sensors, and cloud and precipitation science.

Dr. Brown was a recipient of the NASA Group Achievement Award, in 2004 for his contribution to the UMICH/GSFC Lightweight Rainfall Radiometer.



Erich Schlecht (Member, IEEE) received the B.A. degree in astronomy and physics and the M.S. degree in engineering physics from the University of Virginia, Charlottesville, VA, USA, in 1981 and 1987, respectively, and the Ph.D. degree in electrical and computer engineering from Johns Hopkins University, Baltimore, MD, USA, in 1999.

In 1998, he joined the Jet Propulsion Laboratory, Pasadena, CA, USA, as a member of the Submillimeter-Wave Advanced Technology team. He is currently a senior member of the Engineering Staff. His areas of interest are circuit design and Schottky diode modeling for submillimeter-wave and terahertz LO frequency multipliers and mixers, and astronomical, planetary, and Earth science instruments.

Dr. Schlecht is a member of the IEEE Microwave Theory and Techniques Society and the IEEE Antennas and Propagation Society.

Anders Skalare received the M.S. degree in engineering physics, in 1985 and the Ph.D. degree in applied electron physics, in 1993, both from the Chalmers University of Technology, Gothenburg, Sweden.

He joined the Jet Propulsion Laboratory, in 1993 and has since worked on a variety of high-frequency components and systems between dc and 2.5 THz, including superconducting SIS and HEB heterodyne receivers, and calibration systems. Prior to 1992, he developed SIS receivers for a total of two years at The Netherlands Institute for Space Research (SRON) in Groningen, The Netherlands.



Matthew Bloom received the B.S. and M.S. degrees in electrical engineering from California Polytechnic State University, San Luis Obispo, CA, USA, in 2011 and 2013, respectively.

He joined the Jet Propulsion Laboratory (JPL), Pasadena, CA, USA, as an Electronics Engineer at the Instruments Division in November 2012. Since joining JPL, he has been responsible for the design and delivery of mixed-signal and power electronics hardware for several space instruments, including Insight APSS, surface water, and ocean topography

(SWOT) AMR, Ecostress, Sentinel-6 AMR-C, and M2020 MOXIE.



Violet Torossian received the master's degree in computer science from the University of Southern California (USC), Los Angeles, CA, USA.

She joined the Jet Propulsion Laboratory (JPL), Pasadena, CA, USA, as an Embedded Software Engineering staff in Instruments Division, in June 2001. She has been responsible for delivering embedded flight and ground software systems for flight instruments. She has been involved with many space projects, including MIRI/JWST, MWR/Juno, COWVR, AMR SWOT, AMR-C, MAIA, and PIXL

on M2020. She is currently the Technical Group Supervisor for Instrument Flight Software at JPL/NASA.



John Kanis received the B.S. degree in electrical engineering from the InHolland University of Applied Sciences, Alkmaar, The Netherlands.

He joined the NASA Jet Propulsion Laboratory in Pasadena, CA, USA, in 2015 as a Thermal System Engineer following a 30+ year career in the European Space industry. He has been responsible for the thermal control design in a variety of different projects, such as Earth Orbiting and Deep Space Mission Spacecrafts, re-entry vehicles, optical instruments, radiant cooler, European robot arm, solar arrays, and radiometers.